Journal of Volcanology and Geothermal Research 202 (2011) 117–126

Contents lists available at ScienceDirect

Journal of Volcanology and Geothermal Research

journal homepage: www.elsevier.com/locate/jvolgeores

Deformation of Copahue volcano: Inversion of InSAR data using a genetic algorithm

Maria Laura Velez [a,*], Pablo Euillades [b], Alberto Caselli [a], Mauro Blanco [b], Jose Martínez Díaz [c]

[a] Departamento de Ciencias Geológicas, Facultad de Ciencias Exactas y Naturales, Universidad de Buenos Aires, Argentina
[b] Instituto CEDIAC, Facultad de Ingeniería, Universidad de Cuyo, Mendoza, Argentina
[c] Departamento de Geodinámica, Universidad Complutense de Madrid, Spain

ARTICLE INFO

Article history:
Received 3 August 2010
Accepted 31 January 2011
Available online 13 February 2011

Keywords:
Copahue volcano
SBAS-DInSAR
subsidence
deformation source
genetic algorithm
volcanic–hydrothermal system

ABSTRACT

The Copahue volcano is one of the most active volcanoes in Argentina with eruptions having been reported as recently as 1992, 1995 and 2000. A deformation analysis using the Differential Synthetic Aperture Radar technique (DInSAR) was performed on Copahue–Caviahue Volcanic Complex (CCVC) from Envisat radar images between 2002 and 2007. A deformation rate of approximately 2 cm/yr was calculated, located mostly on the north-eastern flank of Copahue volcano, and assumed to be constant during the period of the interferograms. The geometry of the source responsible for the deformation was evaluated from an inversion of the mean velocity deformation measurements using two different models based on pressure sources embedded in an elastic homogeneous half-space. A genetic algorithm was applied as an optimization tool to find the best fit source. Results from inverse modelling indicate that a source located beneath the volcano edifice at a mean depth of 4 km is producing a volume change of approximately 0.0015 km/yr. This source was analysed considering the available studies of the area, and a conceptual model of the volcanic–hydrothermal system was designed. The source of deformation is related to a depressurisation of the system that results from the release of magmatic fluids across the boundary between the brittle and plastic domains. These leakages are considered to be responsible for the weak phreatic eruptions recently registered at the Copahue volcano.

1. Introduction

Ground deformation is a common phenomenon present in active volcanoes in response to the dynamic of different kinds of magma sources. Surface displacements in volcanic areas are often assumed to be a consequence of pressure changes in a magma reservoir embedded in the crust at a certain depth. These pressure changes can be associated with episodes of eruptive activity. Volcanic activity frequently produces geodetic effects in some combination before, during and after the period of unrest. Therefore, high-precision deformation data are being used to study this volcanic phenomenon.

Techniques for monitoring ground deformation have been improved greatly in recent years, thus active volcanoes currently are monitored not only using terrestrial techniques (e.g., precise levelling GPS) but also using space technology such as Interferometric Synthetic Aperture Radar (InSAR). InSAR provides high quality geodetic data with high temporal and spatial density, characteristics not always present in traditional geodetic techniques. Experience has shown that many real-world surfaces stay correlated for periods ranging from months up to a few years, long enough for most volcanic monitoring purposes, even in areas of sparse-to-moderate vegetation (Dzurisin, 2006). With InSAR, entire volcanic arcs can be surveyed, and magma movements can be detected even beneath volcanoes with no other sign of activity (Pritchard and Simons, 2004b and references therein).

The Copahue volcano (37° 45.35′ S, 71° 11′ W, summit elev. 2997 m) is one of the most active volcanoes in Argentina. The volcano summit has nine craters aligned at N 60° E; the eastern-most crater is presently active and filled with a 200 metre diameter acid hot lake (Varekamp et al., 2001; Caselli et al., 2005). Recent eruptions have been reported in 1992, 1995 and 2000. All these eruptions were characterised by moderate central vent explosive activity (mainly phreatic eruptions). The last eruptive cycle is considered to be its most vigorous activity in the past century because it involved both ash and gas emissions. The villages of Copahue and Caviahue are located 4 km and 9 km from the volcano, respectively. A ski resort and a thermal spa, located in the Caviahue–Copahue area are touristic attractions that are known world-wide. The high vulnerability and the hazards imposed on this area by the volcano enhance the importance of monitoring and the necessity of studying this volcanic system.

The Copahue volcano has been studied using seismic and geochemical data since 2003 (e.g., Caselli et al., 2005; Ibañez et al., 2008; Agusto et al., 2010); however, detailed ground deformation studies have not been performed previously. Moreover, there is no

* Corresponding author at: Permanent address: Universidad de Buenos Aires, Facultad de Ciencias Exactas y Naturales, Departamento de Ciencias Geológicas, Int. Güiraldes 2160, Pabellon II, Ciudad Universitaria, C1428EHA, Buenos Aires, Argentina. Tel.: +54 1145763300x420, +54 1151589333 (Mobile); fax: +54 1145763351.
E-mail address: lvelez@gl.fcen.uba.ar (M.L. Velez).

0377-0273/$ – see front matter © 2011 Elsevier B.V. All rights reserved.
doi:10.1016/j.jvolgeores.2011.01.012

information about the behaviour of this volcanic system before, during and/or after eruptive episodes.

In this work, ground deformation was studied at the CCVC from ENVISAT radar images using the Differential Interferometric Synthetic Aperture Radar technique (DInSAR). Analysing and inverting the InSAR data contributed to a better understanding of the behaviour of this volcanic system. The observed deformation can be explained using two different source models that fit the surface displacements: a point pressure source (Mogi, 1958) and an ellipsoidal source (Yang et al., 1988). Model parameters were searched by inversion using a genetic algorithm (GA) as an optimization method. Results from the inversion were interpreted taking into consideration the available information from seismology, geochemistry and geothermal research. A variety of sources of information were used to achieve a better characterization of the magmatic–hydrothermal system that feeds the volcano and to explain the origin of the observed surface deformation.

2. Geological setting

The CCVC is comprised of the Caviahue caldera and the Copahue stratovolcano (Fig. 1). This complex is located in the Southern Andean Volcanic Zone (33.3°–46°S) and straddles the border between Argentina and Chile, approximately 30 km east of the late Pleistocene–Holocene N–S to NNE-trending volcanic arc (Melnick et al., 2006). Structurally, the CCVC is located within a first-order morphotectonic transition zone between the high and broad Central Andes (3 km to 4 km mean elevation, up to 800 km wide) and the narrow and low (~1 km mean elevation, 300 km wide) Patagonian Andes (Groeber, 1921).

The Caviahue caldera is a square-shaped depression of approximately 20 km × 15 km, defined as a transtensional pull-apart, intra-arc basin due to the local stress field generated in the area of interaction of two fault systems: the Liquiñe–Ofqui Fault Zone (LOFZ) and the Antiñir Copahue Fault Zone (ACFZ). The LOFZ is a 1000 km strike slip fault generated as a consequence of the strain partitioning produced by the oblique subduction of the Nazca plate beneath the South American plate (Hervé and Thiele, 1987; Lopéz Escobar et al., 1995; Cembrano and Lavenu, 1997). The northern segment of the LOFZ ends at the southern side of Caviahue caldera through several splays, Lomin fault being the major one (Fig. 1). The ACFZ is a thrust system that begins at the latitude of the Caviahue caldera and is responsible for its development (Folguera and Ramos, 2000; Folguera et al., 2004; Melnick et al., 2006). The main features of quaternary tectonic activity into the caldera are: the W–NW Trolope and Caviahue grabens that were associated with a last pulse of extension at the caldera and the Chancho-co positive flower structure (Fig. 1). The Chancho-co structure has an approximately NE direction, and it is flanked by nearly vertical faults (Folguera et al., 2004).

Five geothermal fields are recognised in the region, showing manifestations of *boiling pools* and *bubbling pools* with temperatures reaching up to 96 °C and fumaroles that reaches up to 135 °C (Agusto et al., 2007). The Las Maquinas, Las Maquinitas, Copahue and Anfiteatro thermal areas are located northeast of the volcano and appear to be controlled by the northeast structures. The Chancho-co geothermal field is located on the northern flank of the volcano, in close proximity to the volcanic–hydrothermal system.

The Copahue volcano is an active andesitic to basaltic–andesitic stratovolcano nested on the western rim of the Caviahue caldera. Volcanic activity at this edifice began at approximately 1 Ma; however, since the Upper Pleistocene and postglacial period, activity has consisted mainly of effusive emissions of andesitic lava flows and only a few explosive episodes during the Holocene that generated at least 6 ash flows (Muñoz and Stern, 1988; Linares et al., 1999; Naranjo and Polanco, 2004).

During the last 250 years, Copahue eruptions have been weak phreatic and phreatomagmatic types (VEI ≤ 2), and only diluted lahars generated in the 1992 eruption have been partially preserved (Delpino and Bermúdez, 1993). Recent eruptions have been reported in 1992, 1995 and 2000, apparently caused by the interaction of overheated rock with groundwater influx above the magma chamber (Naranjo and Polanco, 2004). As the ascending heat flow melts the ice cap and snow, an acid crater lake is formed. For that reason, a high volume of water vapour accompanied all of the last eruptions. The last eruptive cycle involved ash and gas emissions, and it is considered to be Copahue's most vigorous activity in the past century.

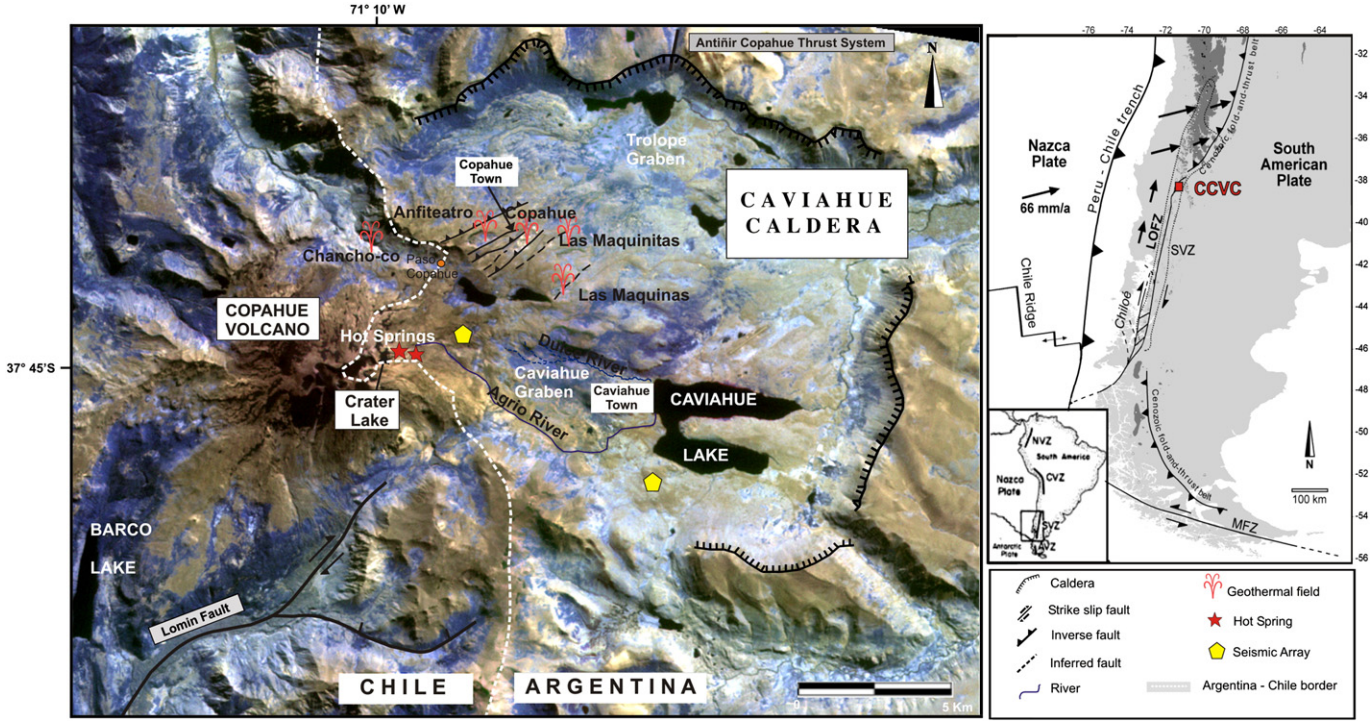

Fig. 1. Location map of the Caviahue–Copahue Volcanic Complex showing the mail structural features, geothermal fields and seismic arrays.

3. InSAR analysis

DInSAR is a geodetic technique used to detect and monitor subtle ground displacements associated with volcanoes, such as dome growth, subsidence and flank destabilisation (Dzurisin and Lu, 2006). The technique is attractive because it allows accurate measurements of the crustal deformation features over an extended area (Rosen et al., 2000) at relatively low cost. Furthermore, by combining a set of SAR scenes acquired over a specific period of time, proper characterization of the spatial and temporal deformation patterns can be achieved.

We processed data from the CCVC area by using the well known Small Baseline Subsets (SBAS) DInSAR technique implemented by Berardino et al. (2002). We modified that implementation to ingest ENVISAT-ASAR data. The main advantage of this approach is that it allows maximisation of both the use of available scenes and the spatial coverage of the solution, even in low coherence regions. It relies on constructing interferograms between scenes whose temporal and perpendicular orbital separation is small and inverting them to obtain displacement time series. The singular value decomposition method is used to link independent data subsets separated by large baselines. The SBAS technique has been broadly validated, and a quantitative study of its effectiveness can be found in Casu et al. (2006).

The employed dataset is composed of 18 scenes acquired by the ENVISAT ASAR sensor in ascending orbit and 14 scenes acquired by the same sensor in descending pass. Acquisition mode is IS2 (23° look-angle) in all cases. The two datasets cover almost the same time period: 12/2002–11/2007 and 12/2002–04/2007, for ascending and descending acquisitions, respectively. A detailed list of the employed scenes is shown in Tables 1. Note that the scenes were mainly acquired between November and May, the southern hemisphere summer season. Winter scenes had to be discarded because of severe coherence loss due to snow cover.

Table 1
(A) Ascending pass ENVISAT scenes (track 261), (B) descending pass ENVISAT scenes (track 239).

Orbit	Day	Month	Year
A			
4323	28	December	2002
5325	8	March	2003
5826	12	April	2003
8832	8	November	2003
9333	13	December	2003
9834	17	January	2004
10,335	21	February	2004
11,337	1	May	2004
14,343	27	November	2004
15,345	5	February	2005
15,846	12	March	2005
19,353	12	November	2005
19,854	17	December	2005
20,355	21	January	2006
20,856	25	February	2006
21,357	1	April	2006
29,373	13	October	2007
29,874	17	November	2007
B			
4301	26	December	2002
5303	6	March	2003
5804	10	April	2003
8309	2	October	2003
8810	6	November	2003
9812	15	January	2004
10,814	25	March	2004
11,315	29	April	2004
11,816	3	June	2004
14,321	25	November	2004
14,822	30	December	2004
15,323	3	February	2005
25,343	4	January	2007
26,846	19	April	2007

The ascending and descending datasets allowed us to calculate 43 and 29 interferograms, respectively, by using SBAS constraints in the spatial and temporal baseline imposed on the data pairs. The selected constraints are a spatial baseline no longer than 300 m and a time baseline no longer than 1500 days (approximately 4 years). Furthermore, precise orbital information and a Shuttle Radar Topography Mission (SRTM) DEM were used to estimate the topographic component of the differential phase. All the SBAS-DInSAR products, that is, deformation time series and mean velocity of deformation maps were calculated following a complex multilook operation with 4 looks in range direction and 20 looks in azimuth direction. The resulting pixel has a dimension of approximately 100 m × 100 m. Mitigation of atmospheric artefacts was achieved based on the observation that a typical atmospheric signal shows high correlation in the spatial domain and low correlation in the time domain (Hanssen, 2001). A series of filters in cascade, previously described by Berardino et al. (2002), was employed to remove it.

An estimation of the quality of the results is given by the temporal coherence map, which was calculated as has been described by Tizzani et al. (2007). Thus, pixels with temporal coherence values under 0.7 were considered as unreliable and masked out of the solution.

Fig. 2a and b shows the mean deformation velocity obtained by applying the SBAS technique on both datasets. They have been computed with respect to a reference point located in the northern border of the Caviahue caldera, indicated by a triangle in the figures. The results have been geocoded and superimposed over a hill shaded DEM of the processed area. Note that low coherence, and thus masked out areas from the results are closely related to layover and foreshortening effects in a mountainous region and all year snow cover. The last phenomenon is particularly important in the southern flank of the Copahue volcano.

Our results show that there is one noticeable oval-shaped deflation feature whose location, which is partially coincident with the Copahue volcano edifice, also extends north-eastward over the Chancho-Co elevation. The availability of ascending and descending geometry allows not only for the calculating of the Line-Of-Sight (LOS) projected components of the deformation, but also allows for the obtaining of a picture of vertical and east–west displacement components. As has been previously shown by Lundgren et al. (2004) and Borgia et al. (2005), the difference of ascending and descending velocity maps over common coherent pixels cancels their vertical and north velocity vectors and shows surface velocities in the east–west direction (Fig. 2c). However, their sum shows mostly vertical velocities (Fig. 2d). This simple calculation is valid because both ascending and descending pass look angles are equal. It gives only a picture of the direction of displacement but not the real magnitudes, which can be calculated by applying a calibration factor that considers the acquisition geometry. In our case, the sum-and-difference methodology allowed us to confirm the nature of the observed deformation, i.e. a deflation bowl.

Deformation time series are also presented (Fig. 3) as extracted at three relevant points whose locations are highlighted in Fig. 2. Greater displacement is found at the summit time-series where, both ascending and descending looks show a deflation trend over the studied time span (5 years) of approximately 2 cm/yr LOS projected. The time-series extracted at Copahue village shows similar behaviour except for the displacement rate, which is approximately 0.5 cm/yr. The last time-series is located at Caviahue village and shows no deflation trend, however, it does indicate a seasonal behaviour that remains unexplained but could be related to Agrio lake water level dynamics.

As has been demonstrated by Doin et al. (2009), vertical stratification can occur if the distribution of scenes is not equal in representing all weather conditions. In this case, the atmospheric

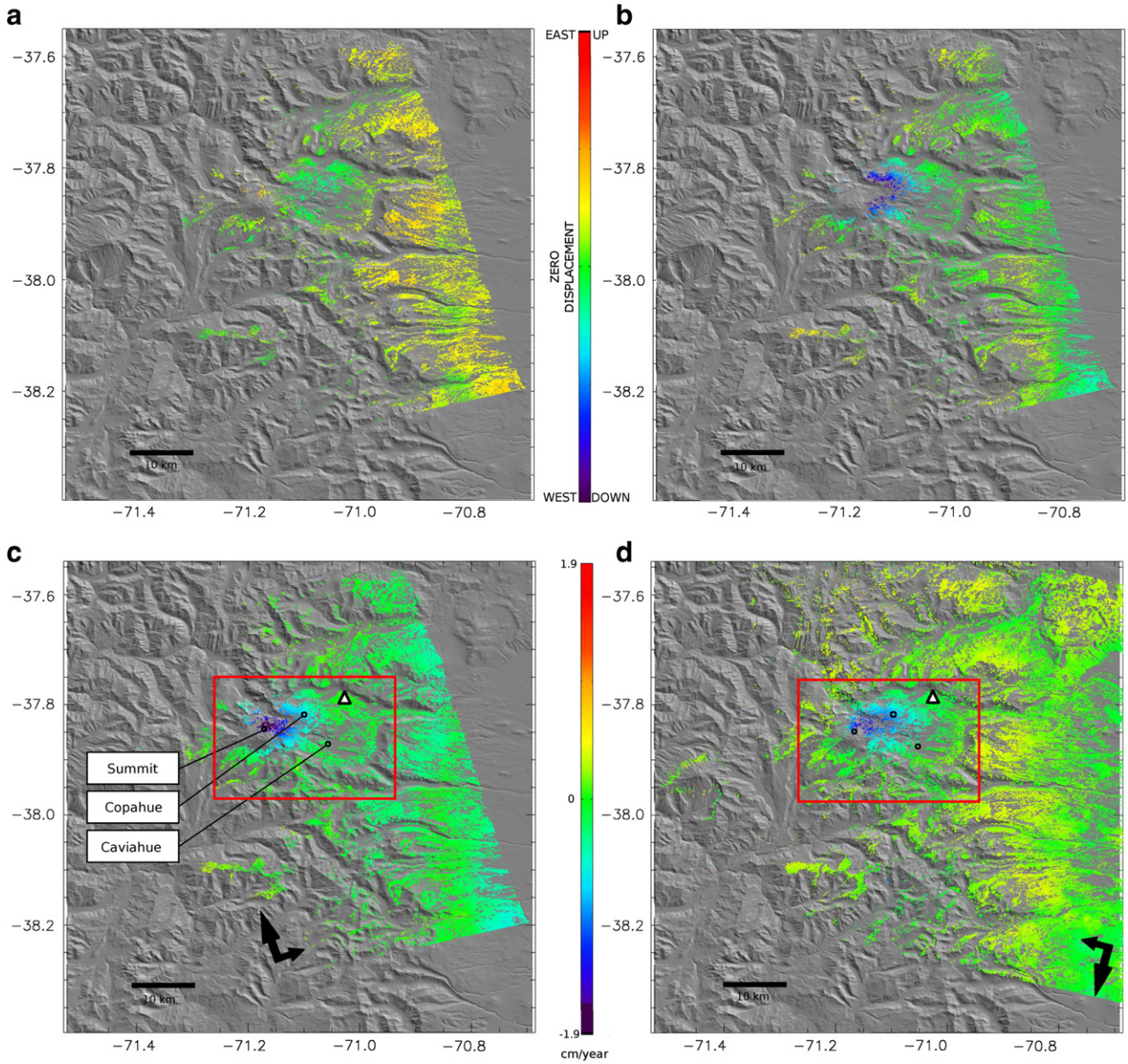

Fig. 2. Mean deformation velocities map (a) ascending pass (b) descending pass. White triangles show the location of the reference point where the deformation amount is zero. Red boxes limit the area where height versus displacement statistics were computed (Fig. 4). Deformation components (c) east–west direction and (d) vertical.

signal compensation based in low pass filtering can be of scarce utility. As previously explained, the time distribution of scenes in our case, is biassed toward the season period between November and May. Thus, we analysed the correlation between deformation velocity and topography, as shown in Fig. 4. We remark that some degree of correlation is expected because the main deformation centre is naturally located more or less under the main volcano edifice, but the shape of the subsidence bowl clearly extends outside the edifice itself. Plots in Fig. 4, corresponding to mean velocity of deformation versus elevation, clearly show two different behaviours: (1) a bulk of pixels with velocity at approximately 0 cm/yr and elevation between 800 m and 2500 m where the two variables are almost not correlated; (2) a group of pixels with velocities between 0 cm/yr and −1.8 cm/yr and elevations between 1500 m and 2300 m where velocity and elevation are well correlated. This second group of pixels is located in the main volcano edifice where deformation is maximum; therefore, correlation in deforming pixels can be explained as a consequence of its location. Although atmospheric influence cannot be completely discarded, this analysis enables us to infer that, in this case, vertical stratification is not a problem for the interpretation of results.

4. Inverse modelling

The main objective of this section is to model InSAR deformation data using analytical solutions based on a single source in a homogeneous half-space. These idealised mathematical models provide a quantitative estimation of the characteristics of the source responsible for the observed deformation, determining its position and geometry. Two analytical models of pressurised sources were used: a point source or Mogi source and an ellipsoidal source. These models were implemented within a GA as an inversion method and provide a valid instrument for understanding general features of volcanic activity.

Ground deformation models are highly non-linear and characterised by a great number of parameters. Therefore, the inverse numerical problem could be difficult to solve by applying methods based on a linearization approach. In this paper, an optimization approach based on

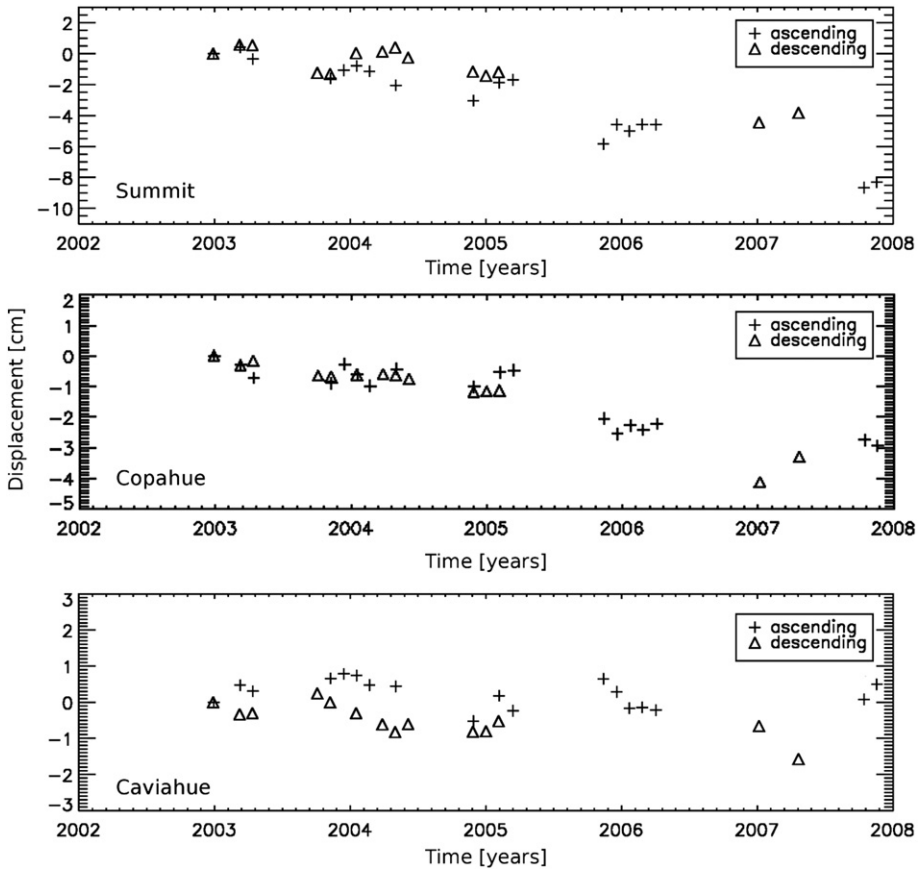

Fig. 3. Displacement time-series extracted at three relevant points: Copahue volcano's summit, Copahue and Caviahue villages.

the use of a GA (Holland, 1975; Goldberg, 1989) was considered to deal with the inverse problem. The aim of this method is to estimate the best fit parameters of the source of deformation (geometry, pressure change, location, depth, etc.). We implement the GA optimization strategies based on the simulation of natural laws to obtain the best solution. These methods search the solution space of a function through the use of simulated evolution, that is, the survival of the fittest philosophy (Fig. 5). In general, the fittest individuals of any population tend to reproduce and survive, thus improving successive generations. However, inferior individuals can, by chance, survive and also reproduce. Because of their initial random and progressively more deterministic sampling of the parameter "space", these algorithms offer the possibility of efficiently and relatively rapidly locating the most promising regions of the solution space (Michalewicz, 1992).

The parameters to be inverted are coded as genes; each gene represents a possible solution to the problem. A large population of genes is searched until the optimal solution is found. The algorithm starts with an initial range of parameters and progressively modifies the solution through several operators, such as selection, crossover and mutation. These operators are used to create new solutions based on existing solutions in the population (Goldberg, 1989). The GA works according to the selection rules as defined by the laws of evolutionary genetics. The algorithm seeks the "fittest" model, i.e., the model that produces solutions to the given problem closest to the observed measurements. The fitness function (F) used to invert the deformation data is:

$$F = \sqrt{\frac{\sum (Um - Ui)^2}{length(Um)}}$$

where Um is the calculated deformation from the model, and Ui is the measured InSAR deformation. To minimise this function and convert this expression to a continuously increasing function, the equation used is $\max f = 1/F$.

The GA moves from generation to generation selecting and reproducing parents until a termination criterion is met. The most frequently used stopping criterion is to specify a maximum number of generations, in this case, 1000.

The two analytical models used have some common features: both are embedded in an elastic homogeneous Poissonian half-space ($\nu = 0.25$, i.e. $\lambda = \mu$) and the rigidity modulus was estimated to be 30 GPa.

Initially, the Mogi model was used, which is the simplest analytical solution for a point-like source in a homogeneous half-space with free-surface (Mogi, 1958; Dzurisin, 2006). It is characterised by only 4 parameters (the source strength and the coordinates of its centre). Therefore, it is generally used when data are scarce, when it shows axial symmetry or as a test model before implementing more realistic numerical models. The mathematical expressions used were derived by Sasai (see Nunnari et al., 2005), where λ and μ are Lamè constant, and C is the nucleus strain. Assuming that the radius (α) is small compared with the depth (d), the nucleus strain can be computed as: $C = -1/2\alpha^3 \Delta P$.

In the Mogi source approximation, the radius of the source cannot be separated from the pressure change (ΔP), and there is also a limiting α/depth condition. A second model was used to calculate the size of the cavity being depressurized and the decrease in pressure; they were estimated independently. An ellipsoidal source model was tested that considers the analytical equations derived by Yang et al. (1988). This source model consists of an arbitrarily oriented spheroidal cavity of finite dimensions embedded in an elastic half-space.

As the larger deformation effects are visible centred at the volcano, it was decided to use only this portion of the SAR image. Working with a smaller area simplifies the inversion process by reducing the

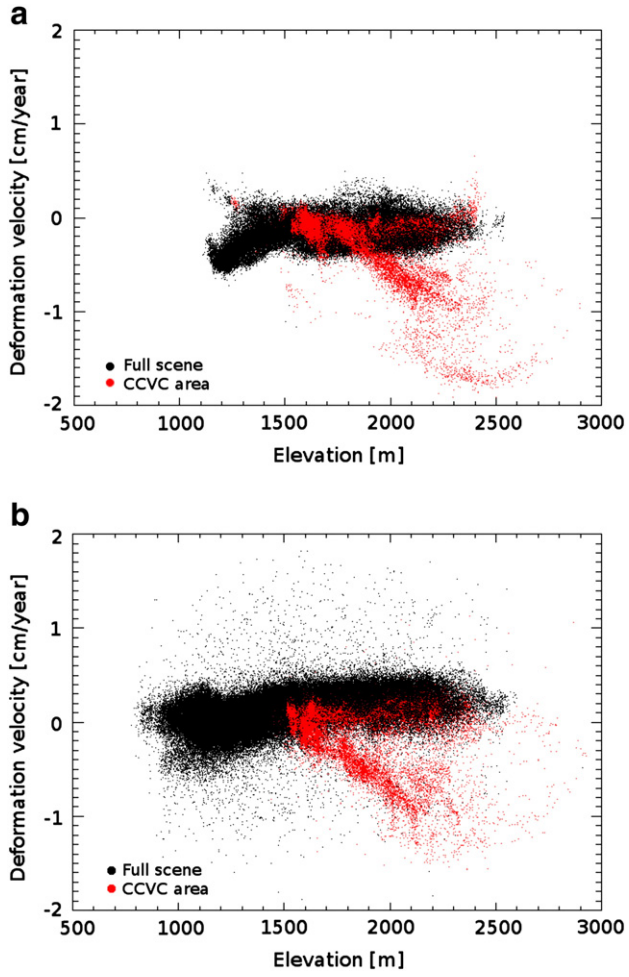

Fig. 4. Correlation between mean velocity of deformation and elevation; (a) ascending pass, (b) descending pass. Calculation was performed by using the whole area (black dots) and the area enclosed by the red box in Fig. 2 (red dots).

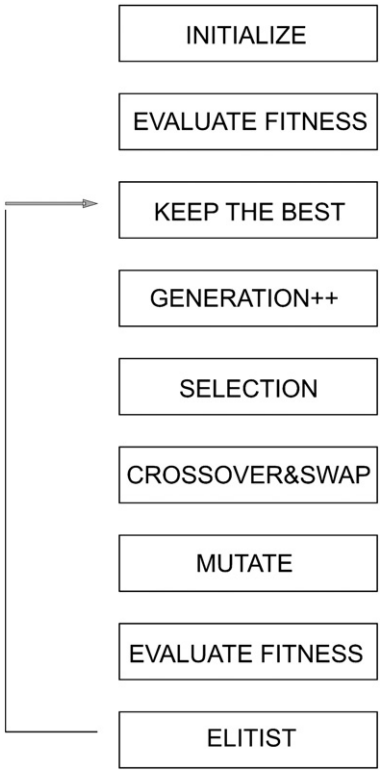

Fig. 5. Diagram of genetic algorithm (Tiampo et al., 2000).

computational effort. The equations of the models and the GA optimization method were programmed as MATLAB codes. The data vector chosen for the inversion is the observed LOS displacements, and the size of the original InSAR ascending data set is 12,910 pixels. The required input data are the elastic constants (Poisson's ratio and rigidity modulus) and the initial range of the parameters to be estimated.

5. Results

The inversion approach described in the previous section was performed to find the optimal parameters for the source. Initially, the subsidence at the Copahue volcano was modelled with a Mogi source, four parameters were estimated: latitude, longitude, depth and radius (Table 2). $\Delta P/G$ was considered a constant at approximately 10^{-3} to calculate an approximate equivalent cavity volume change. A pressure decrease on the spherical cavity produces a decrease in the cavity radius by $\Delta\alpha$ (McTigue, 1987) where $\Delta\alpha = \frac{1}{4}\Delta P/G\alpha$. The volume decrease from the decrease in ratio is $\Delta V \approx \Delta P/G\pi\alpha^3$ (Table 2). This volume change considers only the mechanical properties of the surrounded half-space and is not equivalent to magma volume. Modelling results indicate that the source is located in partial coincidence with the volcano edifice, slightly displaced to the northern flank. The mean depth is approximately 4 km, and the radius change is approximated 500 m thus producing a mean volume decrease of the sphere of about 0.0015 km^3/yr (Fig. 6a). Similar values were obtained by Fournier et al. (2010) from an inversion of two interferograms.

Secondly, we inverted the same data by using an ellipsoidal source. The resulting displacement field is a function of the pressure change (ΔP), the ellipsoidal geometry and its orientation (semi-major and semi-minor axis, depth, dip angle, azimuth angle of the major axis and location). The volume change (ΔV) caused by a pressure change in the ellipsoidal cavity is (Tiampo et al., 2000) $\Delta V = (\Delta P/\mu) * \pi ab^2$ where **a** is the semi-major axis and **b** is the semi-minor axis of the ellipse (Table 2).

The location of the best fit ellipsoidal source (Fig. 6c) is approximately the same as the one estimated by the point pressured source. The mean depth of the source is slightly lower (3900 m), the semi-major and semi-minor axes are about 2000 m and 300 m, respectively. The best fit results were obtained with an oblate ellipsoid; volume change was calculated to be about 0.0013 km^3/yr, slightly lower than that obtained with the Mogi source.

Despite the good fit, some residuals were identified as shown in Fig. 6b and d. The origin of this unmodelled subsidence could be related to the unconsidered topography, the different mechanical properties of the area or the geometry of the sources tested. The planar surface of an elastic half space is not considered a good match to the high relief of volcanic regions (Dzurisin, 2006). This could lead to an overestimation of some parameters (e.g., volume change). Work is in progress to overcome these drawbacks; however, these models represent the first approximation of the source responsible for ground deformation at this particular volcanic system.

According to model results, at first sight, the ellipsoidal source appear to be a better fit with the deformation data, showing smaller residuals (Fig. 6). However, a sensitivity analysis was performed in order to better evaluate the results of the GA inversion for each source.

Following the methodology proposed by Tiampo et al. (2004), the test was performed running the inverse model taking into consideration the different ranges for the parameters under study. In each case, one parameter was varied while the others remained fixed. For each inverted parameter, the distribution of potential solutions versus

Table 2
Best fit parameters for inverse modelling.

Mogi source					
Latitude (°)	Longitude (°)	Depth (km)	Radius (m)	ΔV (km^3/yr)	
−37.8373	−71.1764	4.136	531.23	−0.0015	
Ellipsoidal source					
ΔP (MPa)	**a** (km)	**b** (km)	x0 (°)	y0 (°)	z0 (km)	Dip (°)	ΔV (km^3/yr)
−68.722	1.95	0.32	−37.8382	−71.1798	3.917	88	−0.0013

a — semi-major axis.
b — semi-minor axis.
x0–y0–z0 coordinates of the ellipsoid centre.
Dip — angle down from the horizontal.

correct answer (best fit parameter) was studied to quantify the variation in fitness. Results are shown in Fig. 7, in which fitness is plotted against the normalised variable in question.

The sensitivity analysis shows a significantly steeper, peaked and strongly symmetric fitness profile for the x-coordinate in both models and for the α parameter in the point pressure source. An important characteristic is that sensitivity is almost insignificant for the strike of the ellipsoidal source; this is consistent with the results of the best fit ellipsoid geometry, which is an oblate circular-shaped lens with no strike preference. The depth profiles for both models are highly asymmetric suggesting that the inversion will tend to better fit shallow rather than deep sources.

6. Discussion

Surface deformation at active volcanoes is usually assumed to be produced by magmatic sources embedded on the crust at a certain depth. By inverting surface deformation using simple elastic models the source responsible of these displacements was characterised, at least considering its position and general features.

While mechanical heterogeneities affect the pattern and magnitude of ground deformation, we must consider that homogeneous models could produce an erroneous estimation of magma chamber depth and volume change (Manconi et al., 2007). Efforts are being made to overcome these shortcomings; however, the models used were successful in obtaining the first estimations of these important parameters.

An integrated interpretation of the models was achieved taking into consideration the entire volcanic system. This includes not only the existence of a magma chamber but also a zone of plastic behaviour around the chamber and the associated active hydrothermal system (JICA, 1992; Ouimette, 2000; Panarello, 2002; Varekamp et al., 2004,

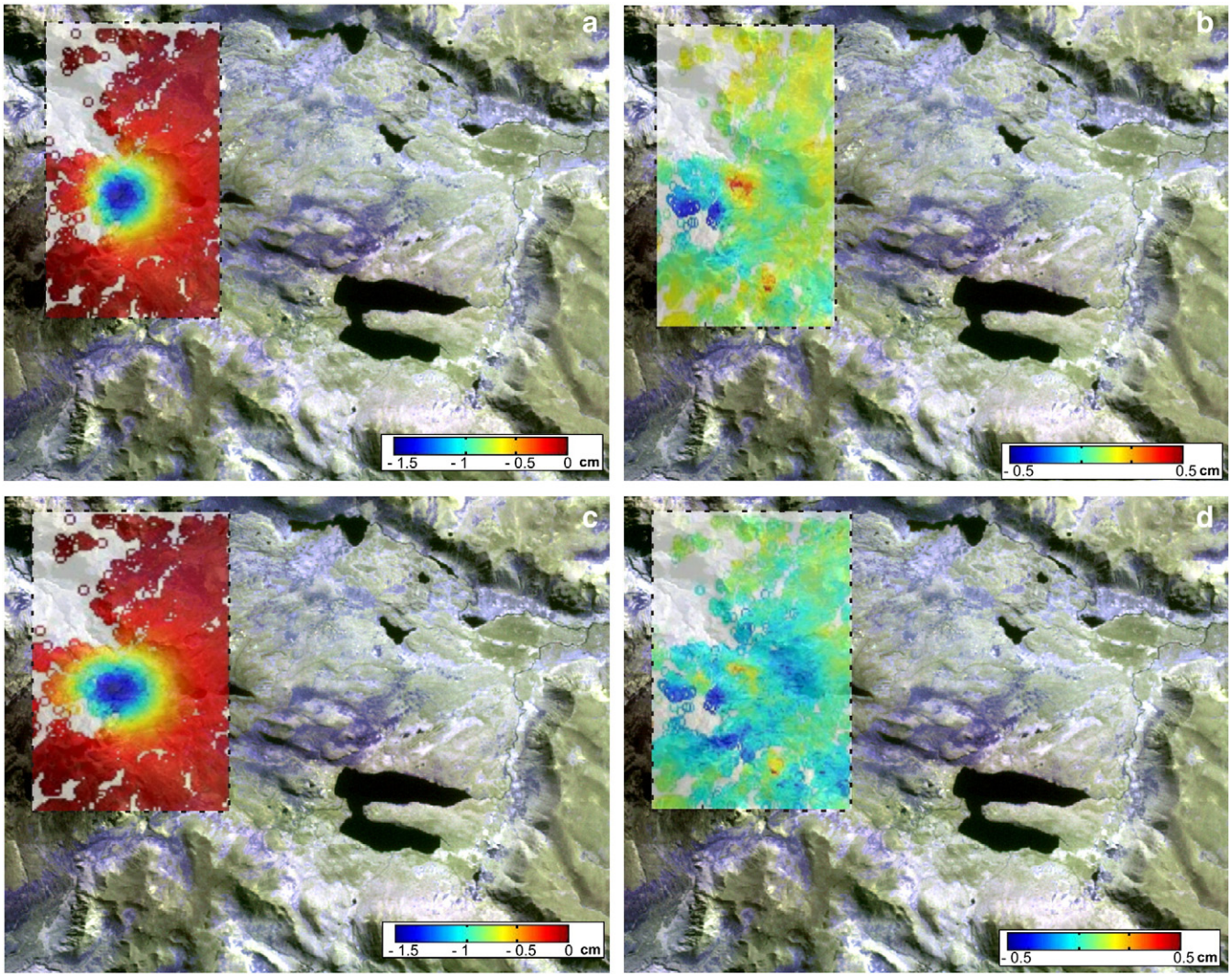

Fig. 6. Panels (a) and (c) show simulated deformation of the models using specific source parameters; best fit solution for Mogi source and ellipsoidal source, respectively. Panels (b) and (c) show the residuals from comparing modelled sources with InSAR deformation measurements (mean deformation map from ascending data set).

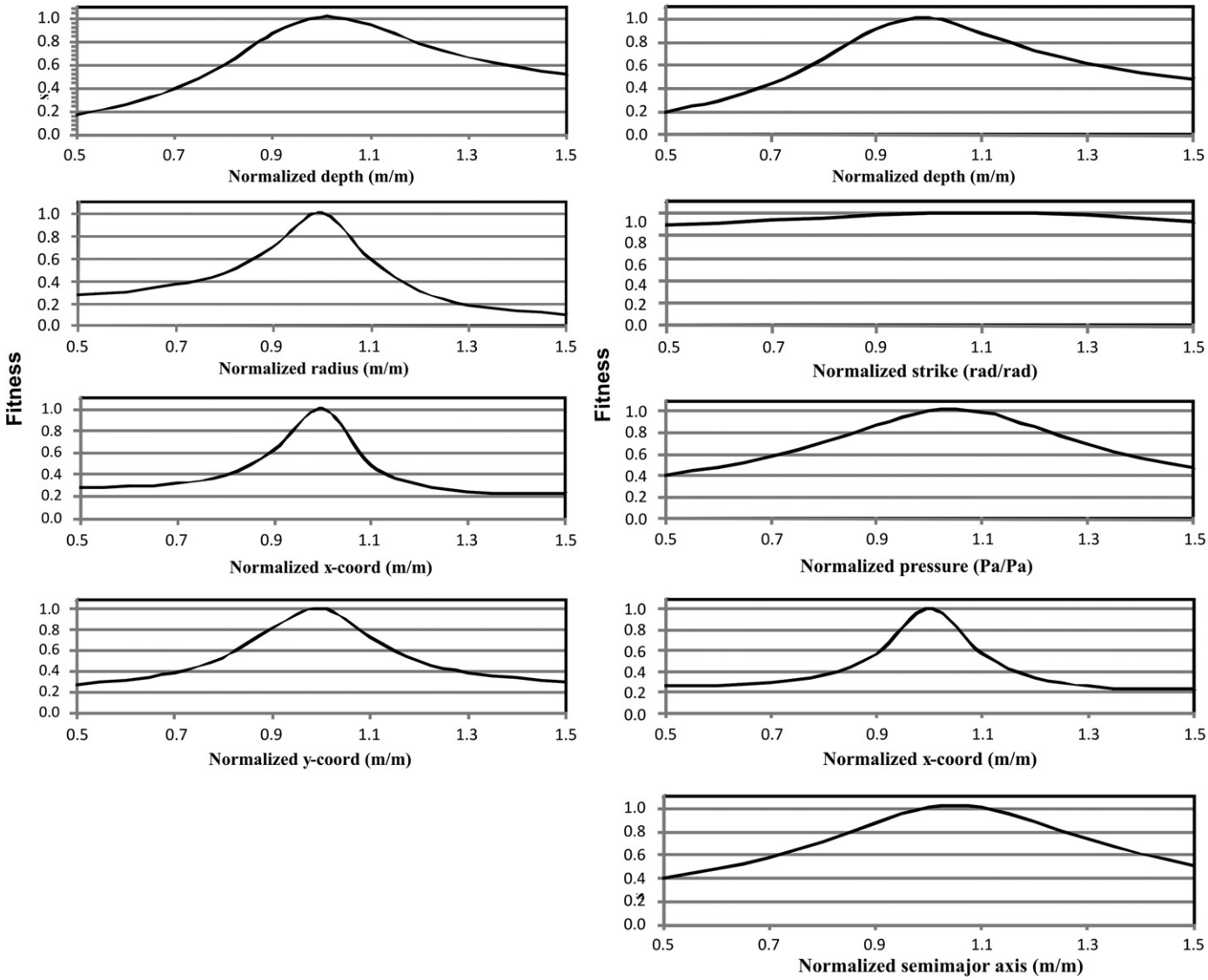

Fig. 7. Sensitivity analysis considering parameters from Mogi and Yang sources. Each parameter is plotted against the best fit solution.

2009). These highly active hydrothermal processes could be responsible for the observed displacements; therefore, relating the source of deformation to a single magma chamber is a considerable simplification that could lead to erroneous interpretations about the system's behaviour.

Several conceptual models have been developed relating the magma chamber to the volcanic–hydrothermal system (Hochstein, 1990; Fournier, 1991, 2006; Hochstein and Sudarman, 1993; Giggenbach, 1997; Cortecci et al., 2001). According to these models and information from geothermal exploration wells, the existence of a brittle–plastic transition zone usually known as a self-sealing zone or carapace, is considered to follow the isotherm of 350–400 °C a few kilometres beneath the surface (Fournier, 2006). This narrow zone or shell of relatively impermeable material separates two very different hydrologic domains. Therefore, an accumulation of aqueous fluids exsolved from the crystallising magma is concentrated beneath this zone. An increase in fluid pressure has been considered as the origin of fracturing and brecciation and thus producing the release of fluids into the hydrothermal brittle zone.

Fig. 8 shows a cross-section of the caldera and a proposed conceptual model of the volcanic system that feeds the Copahue volcano and the geothermal fields. This model is based on the available information from geochemical studies and geophysical surveys performed during geothermal exploration (JICA, 1992) and also consider the deformation data presented in this paper.

Leakages across the brittle–plastic boundary are common phenomena that can range from slow diffusion of non-condensable gases or minor discharges of steam through small fractures quickly resealed up to large explosive events that vent to the surface (Fournier, 2006). Evolved magmatic gases or brines escape into the hydrostatically pressure domain can contribute to ground movements and might be the result of the degassing of brine-filled lenses a few kilometres deep without any input of new magma from deeper in the system. The leakage of these fluids into the brittle domain is believed to be responsible for the deflation observed at the surface of the Copahue volcano.

As shown on Fig. 8, there is no direct connection between the geothermal system and the volcanic–hydrothermal system. As meteoric water flows downward it becomes heated and accumulated in a hot brine geothermal reservoir and returns to the surface through open fractures. Isotopic composition of geothermal fluids and gases suggest a meteoric origin for almost all the geothermal manifestations (JICA, 1992). However, the Chancho-co geothermal field located on the northern flank of the edifice shows a closer relation with the volcanic–hydrothermal system. Therefore, in this case, it could be related to the behaviour of magmatic gases and fluids that tend to rise

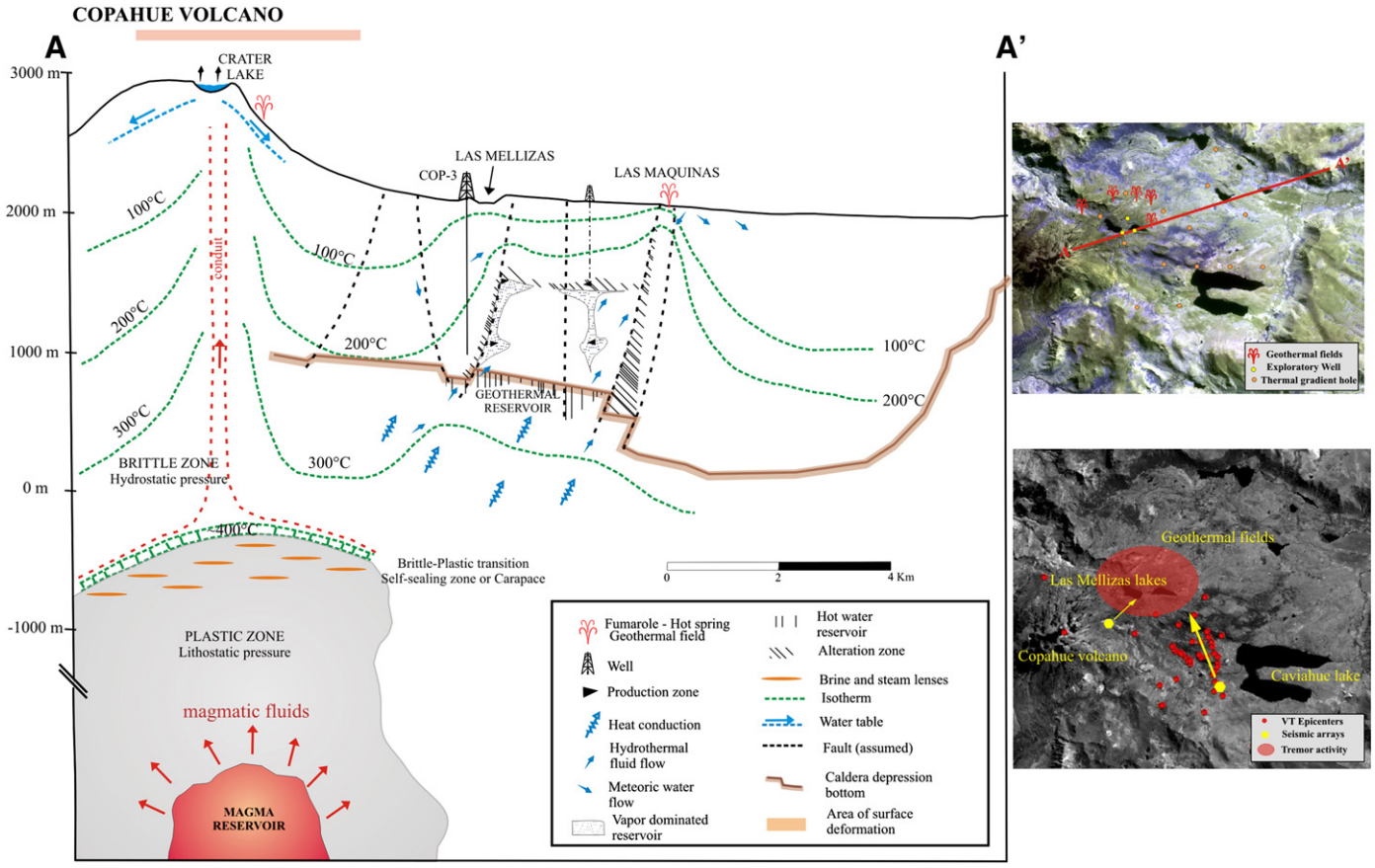

Fig. 8. Conceptual model of the Copahue volcano magmatic–hydrothermal system and the geothermal reservoir.

almost vertically, affecting not only the volcano crater but, the geothermal field on the northern flank, as well.

Seismicity is generally associated with the fracturing of the self-sealing zone. The maximum depth of occurrence of these earthquakes marks the transition between brittle to plastic behaviour in the lithosphere (Fournier, 2006 and references therein). Seismological studies performed at the CCVC registered tremors that were associated with the geothermal fields and volcano-tectonic events at a maximum depth of approximately 3 km located between geothermal fields and Caviahue Lake. These events were associated as a consequence of tectonic activity (Ibañez et al., 2008) that produced the reactivation of small fractures (a few tens of metres); however, they could also be related to periodic fractures of the self-sealing zone. The offset of the registered seismicity with respect to the extension of the magmatic chamber could be a consequence of Coulomb stress changes during deflation periods. Similar to that proposed for the deflation registered before the collapse of the Loihi seamount in Hawaii (Caplan-Auerbach and Duennebier, 2001).

7. Conclusion

Subsidence was observed at the CCVC from 2002 to 2007 at a mean rate of 2 cm/yr and distributed in partial coincidence with the volcanic edifice. The same results were obtained both for the ascending and descending processed images. To discard vertical stratification related to weather conditions, an analysis of deformation velocity versus topography was performed. An inversion of InSAR using simple elastic models and a GA as an optimization method show that most of the deformation at the CCVC can be accommodated by a 4 km depth source located beneath the volcanic edifice with an estimated volume change of approximately 0.0015 km^3/yr.

In the first instance, both models could accurately explain the deflation and suggest similar locations and volume changes. After further analysing the residuals and sensitivity of each parameter, an ellipsoidal source appears to better represent the cause of the deformation.

According to a temporal series, the deflation process seems to be present over the entire period under consideration, although it is not clear when it began and there are no sign of decrease. A complete data set that includes the last eruption in 2000 is being processed to better constrain the deflation event and to analyse the behaviour of the system before, during and after the eruption.

A conceptual model of the volcanic–hydrothermal system centred on the volcano edifice is proposed in coincidence with the surface deformation observed. The existence of a two-phase vapour-brine enclosing the magmatic chamber is also proposed. These brines are prevented from being freely released to the surface by the existence of a self-sealing zone or carapace. This zone corresponds to the brittle–plastic transition and its position has been related to the ~400 °C isotherm. Episodic ruptures of this zone should be responsible for the leakage of magmatic fluids.

This planar ellipsoidal source of approximately 4 km in horizontal extension is considered to be related with the oscillating brittle–plastic boundary where the leakage of brines and steam takes place producing a depressurisation of the system. The conceptual model proposed is compatible with present geochemical, geological and geophysical evidences; however, further geophysical studies (e.g., magnetotellurics) and more realistic models (e.g., viscoelastic rheologies) should be performed to better constrain the location and dimensions of the magmatic–hydrothermal system. Therefore, considering that inflation and deflation periods are mainly the result of hydrothermal processes, deflation (related with the rapid leakage of fluids from plastic rock to brittle regime) could trigger phreatic

eruptions. These mechanisms could explain the last eruptive cycles observed at the Copahue volcano with minor phreatic eruptions registered in 1992, 1995 and 2000.

Acknowledgements

This research was supported by UBACyT X040 project from Universidad de Buenos Aires, project PICT-O 36051 from Agencia Nacional de Promoción Científica y Tecnológica and a Category-1 project from European Space Agency (ESA).

References

Agusto, M., Tassi, F., Caselli, A., Vaselli, O., Tedesco, D., Poreda, R., 2007. Chemical and isotopic features of thermal fluid discharges in the volcano-hydrothermal system of Caviahue–Copahue volcanic complex (Argentina). GEOSUR (International Geological Congress on the Southern Hemisphere, Santiago de Chile — 19/20 November 2007: Actas, vol. 9.

Agusto, M., Tassi, F., Caselli, A., Vaselli, O., 2010. Compositional changes of magmatic–hydrothermal related to anomalous temperaturas at Copahue Crater Lake (Argentina). 6th Congress Cities on Volcanoes (COV), Tenerife, España.

Berardino, P., Fornaro, G., Lanari, R., Sansosti, E., 2002. A new algorithm for surface deformation monitoring based on small baseline differential SAR interferograms. IEEE TGARS 40 (11), 2375–2383.

Borgia, A., Tizzani, P., Solaro, G., Manzo, M., Casu, F., Luongo, G., Pepe, A., Berardino, P., Fornaro, G., Sansosti, E., Ricciardi, G.P., Fusi, N., Di Donna, G., Lanari, R., 2005. Volcanic spreading of Vesuvius, a new paradigm for interpreting its volcanic activity. Geophysical Research Letters 32 (3), L03303.

Caplan-Auerbach, J., Duennebier, F.K., 2001. Seismicity and velocity structure of Loihi Seamount from de 1996 earthquake swarm. Bull Seismol. Soc. Am. 91, 178–190.

Caselli, A.T., Agusto, M.R., Fazio, A., 2005. Cambios térmicos y geoquímicos del lago cratérico del volcán Copahue (Neuquén): posibles variaciones cíclicas del sistema volcánico. Actas del Congreso XVI Congreso Geológico Argentino. La Plata 2005: Tomo I, pp. 332–336.

Casu, F., Manzo, M., Lanari, R., 2006. A quantitative assessment of the SBAS algorithm performance for surface deformation retrieval from DInSAR data. Remote Sensing of Environment, 102, pp. 195–210. doi:10.1016/j.rse.2006.01.23.

Cembrano, J., Lavenu, A., 1997. Coeval transpressional and transtensional magmatic arc tectonic in the Southern Andes. 8° Congreso Geológico de Chile. Antofagasta. Chile, Vol. 3, pp. 1613–1616.

Cortecci, G., Dinelli, E., Bolognesi, L., Boschetti, T., Ferrara, G., 2001. Chemical and isotopic composition of water and dissolved sulfate from shallow wells on Vulcano Island, Aeolian Archipielago, Italy. Geothermics 20, 69–91.

Delpino, D., Bermúdez, A., 1993. La actividad volcánica del volcán Copahue durante 1992. Erupción con emisión de azufre piroclástico. Provincia de Neuquén. XII Congreso Geológico Argentino (Mendoza). Abstracts 4, 292–301.

Doin, M., Lasserre, C., Peltzer, G., Cavalié, O., Doubre, C., 2009. Corrections of stratified tropospheric delays in SAR interferometry: validation with global atmospheric models. Journal of Applied Geophysics 69 (1), 35–50. doi:10.1016/j.jappgeo.2009.03.010.

Dzurisin, D., 2006. Volcano Deformation: New Geodetic Monitoring Techniques. Springer-Verlag, Berlin.

Dzurisin, D., Lu, Z., 2006. Interferometric synthetic-aperture radar (InSAR). [online] Available from In: Dzurisin, D. (Ed.), *Volcano Deformation*. Springer, pp. 153–194. http://dx.doi.org/10.1007/978-3-540-49302-0_5.

Folguera, A., Ramos, V., 2000. Control estructural del volcán Copahue (38°S–71°O): implicancias tectónicas para el arco volcánico cuaternario (36°–39°). Revista de la Asociación Geológica Argentina, Vol. 53, pp. 229–244.

Folguera, A., Ramos, V.A., Hermanns, R.L., Naranjo, J., 2004. Neotectonics in the foothills of the Southernmost Central Andes (37°–38°S). Evidence of the strike-slip displacement along the Antiñir–Copahue fault zone. Tectonics 23 (5).

Fournier, R.O., 1991. The transition between hydrostatic to greater than hydrostatic fluid pressure in presently active continental hydrothermal systems in crystalline rock. Geophysical Research Letters 18 (5), 955–958.

Fournier, R.O., 2006. Hydrothermal systems and volcano geochemistry. [online] Available from In: Dzurisin, D. (Ed.), *Volcano Deformation*. Springer, pp. 153–194. http://dx.doi.org/10.1007/978-3-540-49302-0_5.

Fournier, T.J., Pritchard, M.E., Riddick, S.N., 2010. Duration, magnitude and frequency of subaerial volcano deformation events: new results from Latin America using InSAR and a global synthesis. Geochemistry Geophysics Geosystems 11 (1), Q01003. doi:10.1029/2009GC002558.

Giggenbach, W., 1997. The origin and evolution of fluids in magmatic–hydrothermal systems, In: Barnes, H.L. (Ed.), Geochemistry of Hydrothermal Ore Deposits, 3rd ed. Wiley, New York, pp. 737–796.

Goldberg, D.E., 1989. Genetic Algorithm in Search, Optimization and Machine Learning. Addison-Wesley, Reading, MA.

Groeber, P., 1921. La region de Copahue y su glaciación diluvial. Revista de la Sociedad Argentina de Estudios Geográficos 1, 92–110.

Hanssen, R.F., 2001. Radar Interferometry — Data Interpretation and Error Analysis. [online] Available from: Kluwer Academic Publishers, U.S. http://kluweronline.com.

Hervé, F., Thiele, R., 1987. Estado del conocimiento de las megafallas de Chile y su significado tectónico. Comunicaciones 38, 67–91.

Hochstein, M.P., 1990. Classification and assessment of geothermal resources. In: Dickson, M.H., Fanelli, M. (Eds.), Small Geothermal Resources: A Guide to Development and Utilization: UNITAR/UNDP Centre for Small Energy Resources, Rome.

Hochstein, M.P., Sudarman, S., 1993. Geothermal resources of Sumatra. Geothermics 22, 181–200.

Holland, J., 1975. Adaptation in Natural and Artificial Systems. The University of Michigan Press, Ann Arbor.

Ibañez, J.M., Del Pezzo, E., Bengoa, C.L., Caselli, A.T., Badi, G., Almendros, J., 2008. Volcanic tremor and local earthquakes at Copahue volcanic complex, southern Andes, Argentina. Journal of Volcanology and Geothermal Research 174, 284–294. doi:10.1016/j.jvolgeores.2008.02.005.

JICA (Japan International Cooperation Agency), 1992. The feasibility study on the Northern Neuquen Geothermal Development Project. (Unpublished), Ente Provincial de Energía de la Provincia del Neuquen. 89 pp.

Linares, E., Ostera, H.A., Mas, L., 1999. Cronología Potasio-Argón del complejo efusivo Copahue–Caviahue, Provincia de Neuquén. Revista de la Asociación Geológica Argentina 54 (3), 240–247.

Lopéz Escobar, L., Cembrano, J., Moreno, H., 1995. Geochemistry and tectonics of the Chilean Southern Andes basaltic Quaternary volcanism (37°–46°S). Revista Geológica de Chile 22, 219–234.

Lundgren, P., Casu, F., Manzo, M., Pepe, A., Berardino, P., Sansosti, E., Lanari, R., 2004. Gravity and magma induced spreading of Mount Etna volcano revealed by satellite radar interferometry. Geophysical Research Letters 31 (4), L04602.

Manconi, A.T., Walter, R., Amelung, F., 2007. Effects of mechanical layering on volcano deformation. Geophys. J. Int 170 (2), 952–958. doi:10.1111/j.1365-246X.2007.03449.x.

McTigue, D.F., 1987. Elastic stress deformation near a finite spherical magma body: resolution of the point source paradox. Journal of Geophysical Research 92, 12931–12940.

Melnick, D., Folguera, A., Ramos, V.A., 2006. Structural control on arc volcanism: the Copahue–Agrio complex, South-Central Andes (37°50′S). Journal of South American Earth Sciences 22, 66–88.

Michalewicz, Z., 1992. Genetic Algorithm + Data Structures = Evolution Programs. Springer, New York. 387 pp.

Mogi, K., 1958. Relations between the eruptions of various volcanoes and the deformations of the ground surface around them. Bulletin of Earthquake Research Inst. Univ. Tokyo 36, 99–134.

Muñoz, J., Stern, C., 1988. The Quaternary volcanic belt of the sourthern continental margin of South America: transverse structural and petrochemical variations across the segment between 38° and 39°S. Journal of South American Earth Science 1, 147–161.

Naranjo, J.A., Polanco, E., 2004. The 2000 AD eruption of Copahue Volcano, Southern Andes. Revista Geológica de Chile 31 (2), 279–292.

Nunnari, G., Puglisi, G., Guglielmino, F., 2005. Inversion of SAR data in active volcanic areas by optimization techniques. Nonlinear Processes in Geophysics 12, 863–870 (SRef-ID: 1607-7946/npg/2005-12-863).

Ouimette, A.P., 2000. Hydrothermal processes at an active volcano, Copahue, Argentina. MA. Thesis, Wesleyan Univ., Middletown, CT.

Panarello, H.O., 2002. Características isotópicas y termodinámicas de reservorio del campo geotérmico Copahue–Caviahue, provincia del Neuquén. Revista de la Asociación Geológica Argentina 57 (2), 182–194.

Pritchard, M.E., Simons, M., 2004. An InSAR-based survey of volcanic deformation in the southern Andes. Geophysical Research Letters 31, L15610. doi:10.1029/2004GL020545.

Rosen, P., Hensley, S., Joughin, I.R., Li, F., Madsen, S., Rodriguez, E., Goldstein, R.M., 2000. Synthetic aperture radar interferometry. Proceedings of the IEEE 88 (3), 333–382.

Tiampo, K.F., Rundle, J.B., Fernandez, J., Langbein, J.O., 2000. Spherical and ellipsoidal volcanic sources at Long Valley caldera, California, using a genetic algorithm inversion technique. J. Volcanol. Geothrm. Res. 102, 189–206.

Tiampo, K.F., Fernandez, J., Gentzsch, G., Charco, M., Rundle, J.B., 2004. Inverting for the parameters of a volcanic source using a genetic algorithm and a model for magmatic intrusion in elastic–gravitational layered Earth models. Computer & Geosciences 30 (9–10), 985–1001.

Tizzani, P., Berardino, P., Casu, F., Euillades, P., Manzo, M., Ricciardi, G.P., Zeni, G., Lanari, R., 2007. Surface deformation of Long Valley caldera and Mono Basin, California, investigated with the SBAS-InSAR approach. Remote Sensing of Environment 108, 277–289.

Varekamp, J.C., Ouimette, S.O., Herman, S.W., Bermudez, A., Delpino, D., 2001. Hydrotermal element fluxes from Copahue, Argentina: a “beehive” volcano in turmoil. Geology 29 (11), 1059–1062.

Varekamp, J.C., Ouimette, A., Kreulen, R., 2004. The magmato-hydrothermal system at Copahue volcano, Argentina. In: Wanty, R.B., Seal II, R.B. (Eds.), Proc. Water–Rock Interaction, vol. 11. Bakema Publishers, Leiden, pp. 215–218. 1.

Varekamp, J.C., Ouimette, A.P., Herman, S.W., Flynn, K.S., Bermudez, A., Delpino, D., 2009. Naturally acid waters from Copahue volcano, Argentina. Applied Geochemistry 24, 208–220.

Yang, X.M., Davis, P.M., Dieterich, J.H., 1988. Deformation from inflation of a dipping finite prolate spheroid in a elastic half-space as a model for volcanic stressing. Journal of Geophysical Research 93, 4249–4257.